Journal of Materials Processing Tech. 252 (2018) 421–431

Contents lists available at ScienceDirect

Journal of Materials Processing Tech.

journal homepage: www.elsevier.com/locate/jmatprotec

Numerical study of keyhole instability and porosity formation mechanism in laser welding of aluminum alloy and steel

Lijin Huang[a,b], Xueming Hua[a,b,*], Dongsheng Wu[a,b], Fang Li[a,b]

[a] Shanghai Key Laboratory of Materials Laser Processing and Modification, School of Materials Science and Engineering, Shanghai Jiao Tong University, Shanghai 200240, China

[b] Collaborative Innovation Center for Advanced Ship and Deep-Sea Exploration, Shanghai, 200240, PR China

ARTICLE INFO

Keywords:
Laser welding
Keyhole
Porosity
Aluminum alloy

ABSTRACT

The instability of the keyhole and bubble being captured by solidification interface are the main factors that affect the formation of porosity in laser welding of both aluminum alloy and steel. In laser welding of aluminum alloy, the more violent fluid flow behind the keyhole, the larger depth to width ratio can cause the keyhole more unstable, and susceptive to collapse that can be described as three necessary steps. The much larger solidification rate and longer escaping distance make the bubble easily captured by the solidification interface, and easily combined. All of these reasons contribute to the formation of larger number and size of porosity in laser welding of aluminum alloy. The numerical and experimental results are in good agreement.

1. Introduction

Laser welding is extensively applied to the welding of structured materials, such as aluminum alloy and steel, in today's industrial manufacturing (Olabode et al., 2015). However, keyhole-induced porosity may occur during the welding, which would strongly weaken the joint strength (Yu et al., 2010; Lu et al., 2015). Owing to the great differences in the physical properties between aluminum alloy and steel, keyhole-induced porosity formation is usually expected to be different during laser welding of these two metals.

Matsunawa et al. (2003) used high speed X-radiography to observe the keyhole behavior during the laser welding of AA5083 aluminum alloy, and proposed that the dynamic pressure of metal vapor caused by intense evaporation of hump at the keyhole front wall, would generate dents at the rear wall of the keyhole, and accelerated the instability of the entire keyhole. The same phenomena can be observed in laser welding of steel (Matsunawa, 2001). Tsukamoto et al. (2003) used X-ray imaging system to observe the keyhole variation in 20 kW CO_2 laser welding of steel, and put forward the liquid column model to expound the porosity formation mechanism. Ribic (Ribic et al., 2009) suggested that the pressure equilibrium at the keyhole wall can affect the porosity formation. Courtois et al. (2016) and Meng et al. (2014) indicated the keyhole-induced porosity formation was closely related to keyhole collapse caused by keyhole instability. Based on experimental investigation, valuable information can be acquired to understand the keyhole behavior and porosity formation. However, some useful information is hard to be obtained merely relying on experiments, such as the temperature distribution, the fluid flow field, which are closely related to the porosity formation and amalgamation.

Numerical simulation based on a comprehensive mathematical model can help better understand the process mechanism of laser welding. Many researches have been carried out to model the thermal and stress fields (Xia et al., 2014; Yilbas et al., 2010), and keyhole behavior (Volpp and Vollertsen, 2015; Mueller, 2012) in laser welding. However, few researches focused on modeling the keyhole-induced porosity formation. Zhou and Tsai (2007) developed a 2D mathematical models to systematically discuss the porosity formation in laser welding of 304 standard steels, and found that bubble was formed when the keyhole could not be filled by the molten metal. Zhao et al. (2011) simulated the keyhole phenomena and molten pool in laser welding of stainless steel 304L, and found that the keyhole collapse and shrinkage were the two factors that were responsible for keyhole-induced porosity. Cho et al. (2012) used the adiabatic bubble model to describe the bubble formation and motion during laser welding of low carbon steel. Lin et al. (2017) used numerical process simulations to investigate the effect of weld speed and laser inclination angle on porosity formation in laser welding of AA5182 aluminum alloy.

In this paper, a three-dimensional mathematical model considering the Fresnel absorption and multi-reflection of laser beam is developed to study the keyhole and bubble behaviors during the laser welding of

* Corresponding author at: Shanghai Key Laboratory of Materials Laser Processing and Modification, School of Materials Science and Engineering, Shanghai Jiao Tong University, Shanghai 200240, China.

E-mail addresses: xmhua@sjtu.edu.cn, lijinhuang@sjtu.edu.cn, xmhuasjtu@163.com (X. Hua).

http://dx.doi.org/10.1016/j.jmatprotec.2017.10.011
Received 13 June 2017; Received in revised form 28 September 2017; Accepted 6 October 2017
Available online 09 October 2017
0924-0136/

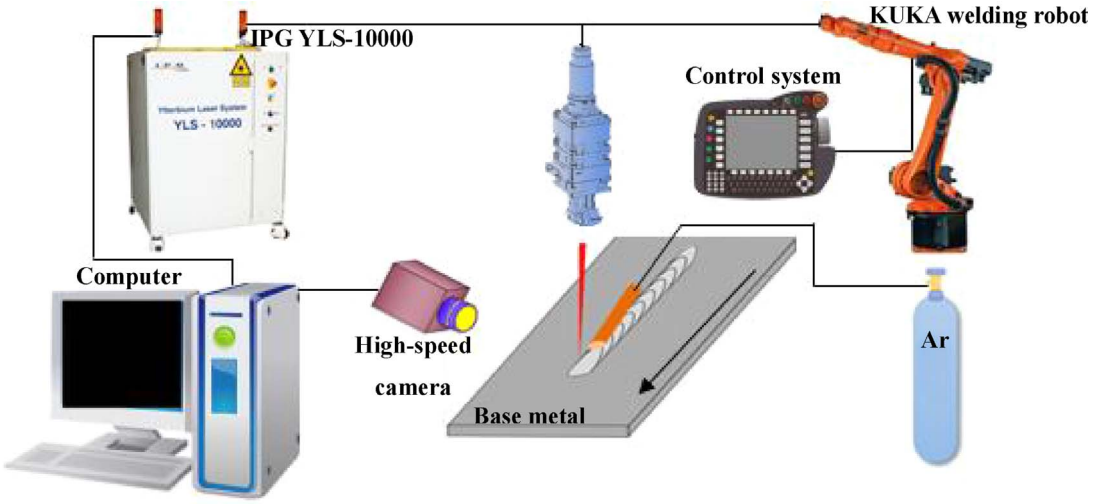

Fig. 1. Diagram of the experimental platform.

aluminum alloy and steel. The keyhole instability and porosity formation mechanism are analyzed. The differences in porosity formation between aluminum alloy and steel laser welding are also illuminated.

2. Experimental procedure

The experimental setup of 10 mm thick 5083 aluminum alloy and Q345 steel are used for the experiments is shown in Fig. 1, and the thermo-physical material properties of the base metal are summarized in Table 1. A fiber laser welding machine (IPG YLS-10000 with a maximum power of 10 kW) is used, and the wavelength of laser beam is 1.07 μm. Prior to welding, the plate is brushed by a stainless steel brush, and then cleaned by acetone. The optical fiber laser is focused on a spot with a diameter of 0.72 mm through a lens with a focal length of 400 mm. A high speed CCD camera is applied to observe the keyhole and weld pool behavior, and a low power laser-assisted light with a wavelength of 640 nm is used as backlight source to illuminate the welding zone to obtain clear images. The welding phenomenon is recorded at a frequency of 5000 frames/s.

The welding was performed at a welding speed of 2 m/min with a laser power of 6 kW. The defocused distance is 0 mm. In order to improve the welding quality, pure argon shielding gas with a flow rate of 20 L/min in an 8 mm diameter is blown into the weld pool at an angle of 45°. The X-ray radiography is carried out to analyze the porosity after welding. The longitude-section along the center line and the cross-section of the samples are observed by optical microscope of Zeiss Stemi2000 after etching in 10% HF.

3. Mathematical model and numerical simulation

Since laser welding involves an intricate multi-physical phenomenon, in present model, some assumptions and simplifications have been considered as follows: (1) fluid flow is assumed to be Newtonian, laminar, and incompressible; (2) the weld shielding gas is neglected; (3) the laser heat source distribution of laser beam is assumed to be Gaussian distribution.

Table 1
Thermo-physical material properties used in simulation .

Nomenclature	Unit	aluminum alloy	steel
Density	$Kg\ m^{-3}$	2660	7830
Specific heat of the solid phase	$J\ kg^{-1}\ K^{-1}$	1050	670
Dynamic viscosity	$Pa\ s$	4.2×10^{-3}	5.9×10^{-3}
Thermal expansion coefficient	K^{-1}	1.5×10^{-4}	4.48×10^{-5}
Solidus temperature	K	847	1688
Liquidus temperature	K	933	1725
Latent heat of fusion	$J\ kg^{-1}$	3.87×10^{5}	2.77×10^{5}
Thermal conductivity	$W\ m^{-1}\ k^{-1}$	90	24.9

3.1. Governing equations

The differential equations governing the weld pool simulation of mass, momentum, and energy are applied to describe the heat transfer, mass transfer, and the melt flow. The Volume of Fluid (VOF) method is used to trace the free surface deformation of the weld pool (Li et al., 2014).

Mass conservation equation:

$$\nabla \vec{V} = 0 \tag{1}$$

where $\vec{V}$ is the velocity vector.

Momentum continuity equation:

$$\frac{\partial \vec{V}}{\partial t} + \vec{V}\nabla\vec{V} = \frac{1}{\rho}\nabla P + \mu\nabla^2\vec{V} + K\vec{V} + F_b \tag{2}$$

where ρ is the fluid density, is kinematic viscosity, K is the drag coefficient, and F_b is body force.

Energy conservation equation:

$$\rho\frac{\partial h}{\partial t} + \nabla(\vec{V}F) = 0 \tag{3}$$

VOF equation:

$$\frac{\partial F}{\partial t} + \nabla(\vec{V}F) = 0 \tag{4}$$

where h is the enthalpy, κ is the thermal conductivity, and T is the temperature.

The energy-temperature relationship can be described by the solid-liquid phase transition model (Ronda and Siwek, 2011).

$$h = \begin{cases} \rho_s C_s T & (T \le T_s) \\ h(T_s) + \Delta H_l \frac{T - T_s}{T_l - T_s} & (T_s < T \le T_l) \\ h(T_l) + \rho_l C_l (T - T_l) & (T_l < T) \end{cases} \tag{5}$$

where ρ_s, ρ_l are solid and liquid density respectively; T_s and T_l are the solidus and liquidus temperature respectively; C_s and C_l are the specific heat of the solid and liquid phases respectively; ΔH_l represent latent heat of fusion.